IEEE Access
Multidisciplinary | Rapid Review | Open Access Journal

Received November 28, 2019, accepted December 20, 2019, date of publication December 31, 2019,
date of current version January 9, 2020.

Digital Object Identifier 10.1109/ACCESS.2019.2963197

A Detailed Reliability Study of the Motor System in Pure Electric Vans by the Approach of Fault Tree Analysis

XIONG SHU[1,3], YINGFU GUO[1], WENXIAN YANG[2], KEXIANG WEI[3], YUN ZHU[3], AND HONGXIANG ZOU[3]

[1]School of Mechanical Engineering, Hunan University of Science and Technology, Xiangtan 411201, China
[2]School of Engineering, Newcastle University, Newcastle upon Tyne NE1 7RU, U.K.
[3]Hunan Provincial Key Laboratory of Vehicle Power and Transmission System, Hunan Institute of Engineering, Xiangtan 411104, China

Corresponding author: Kexiang Wei (kxwei@hnie.edu.cn)

This work was supported in part by the Hunan Province Science and Technology Innovation Program under Grant 2017XK2303, Grant 2019RS2044, and Grant 2019JJ50099, and in part by the Research Foundation of Education Department of Hunan Province, China, under Grant 18B389.

ABSTRACT Attributing to the unique feature of zero carbon emission, electric vehicles (EVs) are attracting increasing interest in recent years, but their reliability, particularly the reliability of their critical components, is still a matter of concern today. In order to address this issue, much effort has been made before to assess the reliability of drive motor in the EVs. However, drive motor and motor controller are logically integrated and requested to work as one system in the EVs. In contrast to the individual reliability analysis of them, the combined assessment of the two parts can provide a more reliable prediction to the reliability of the entire motor system. Moreover, both drive motor and motor controller are composed of multiple components. The structure, type, and characteristics of these components may affect the reliability of the motor system as well. But these issues have not been considered in the previous research. In order to fill this gap of knowledge, the reliability of the entire motor system of pure electric vans that includes both drive motor and motor controller is investigated in this paper. In the research, the theoretical failure rates of subassemblies and components in drive motor and motor controller are predicted first. Then based on the failure rate prediction results, the reliability of the entire motor system (comprising both drive motor and motor controller) is assessed. Based on the assessment results, some interesting conclusions with respect to the most vulnerable subassemblies and components in the entire motor system and the potential disadvantage of existing reliability research are finally obtained. It is deemed that these new findings will be of great significance to the future reliability design and maintenance of pure electric vans.

INDEX TERMS Reliability, electric vehicles, motor system, motor controller, fault tree analysis.

I. INTRODUCTION

Encouraged by financial subsidies and policy dividends, the market of electric vehicles is booming across the world today. The recent survey has shown that China, the UK, the United States, and Germany currently top the world ranking of the sales of pure electric vehicles [1]. Take the Chinese market as an example, total 984,000 pure electric vehicles were sold in China in 2018, which was an increase of 50.8% over the same period of the previous year [1]. It is deemed that pure electric vehicles will replace traditional diesel and petrol vehicles at some point in the near future. For example, it would be 2040 in the UK. This means that there will be many pure electric vehicles running on the road in the following years. That is why their reliability in the application is receiving more concern than ever before.

Broadly speaking, pure electric vehicles can be classified into two categories, i.e. passenger cars and commercial vehicles. Their market share splits are about 80% versus 20%. For example, 788,000 passenger cars and 196,000 commercial vehicles were sold in China in 2018 [1]. In terms of reliability, the practice has shown that the latter is more prone to develop failure in the application, although such a comment has not yet been officially reported before in open literature.

The associate editor coordinating the review of this manuscript and approving it for publication was Lorenzo Ciani.

For this reason, the research in this paper will be focused on investigating the reliability of commercial vehicles. Herein, considering more than 90% of sold commercial vehicles are pure electric vans [1] and the motor system is the most key part in these vehicles, the reliability of the motor system in pure electric vans will be studied in the following.

The motor system in pure electric vans is used to convert the electric energy into mechanical energy to drive the vehicle. Any reliability issue existing in the motor system may lead to dangerous accidents on the road. Therefore, it is essential to investigate its reliability issues, identify the vulnerable parts in the system, and then improve its design based on the investigation results [2], [3]. In order to meet this purpose, much effort has been made before. A detailed literature review has shown that so far, the majority of published works in the relevant area are focused on how to improve the control and fault tolerance performance of motor systems. For example, the fault tolerance performance of multi-phase permanent magnet synchronous motor was investigated in [4] with the aid of a multi-level Markov model; the similar research on motor drives was also conducted in [5] by using the Monte Carlo method in order to get better fault-tolerance mechanisms. The reliability of automated guided vehicles' (AVGs) control system was studied in [6] by using a combined fault tree and Petri net approach; the research was further improved by the authors in [7] through introducing genetic algorithm method into the maintenance strategy optimization. Fault classification method and fault-tolerant control strategies were adopted in [8] in order to improve the dynamic performance and control stability of electric vehicles. The reliability of drive motor and electronic converter for power supply was also studied by scholars. For example, the reliability of the drive motor of EVs was studied in [9], [10] by using a combined fault tree and Petri net approach, and the fault logical causes by the winding insulation and bearing with higher fault rate were investigated in [11] by the approach of fault tree analysis. The reliability of bidirectional DC/DC converters of EVs was studied in [12]; the age and life of power converter components were estimated in [13] based on a survey, and so on. However, it is noticed that in previous research, the reliability study was mainly focused on the analysis of drive motor, and the reliability issues in the motor controller were rarely discussed. This may lead to unreliable research conclusions due to the fact that the drive motor and motor controller are logically integrated. They are always requested to work as one system and cannot be dealt with individually. A combined reliability assessment of the two parts will provide a more reliable prediction of the reliability of the entire motor system. However, such detailed reliability research of the entire motor system has not been conducted before. This motivates the research of this paper. Moreover, both drive motor and motor control are composed of multiple components. The structure, type, and characteristics of components may also affect the reliability of the entire motor system. However, this has not been considered before either. The purpose of this research is to fill these gaps of knowledge by looking into the reliability issues of all subassemblies and components in both the drive motor and motor controller. The outcome of this research should be a good complement to the current knowledge of electric vehicles and it will also bring benefits to the emerging electric vehicle industry.

Fault tree analysis, an effective methodology for conducting reliability and safety assessment, has been extensively used to investigate the reliability issues in various systems. For example, the potential failures of wind turbine were qualitatively and quantitatively evaluated by using the fault tree analysis method in [14], and it was found that the majority of floating turbine failures are due to marine conditions, salt-spray, and high wind speed; the fault tree analysis method was further improved in [15] in order to adapt to performing the qualitative analysis of complex systems containing multi-component systems; the dynamic fault tree analysis model was developed in [16] to determine the average maintenance period of a floating wind turbine; the dynamic fault tree models were developed in [6] and [17] for assessing the reliability of a fault-tolerant control system and a vehicle guidance system in unmanned aerial vehicles; and so on. In view of these previously successful applications of fault tree analysis, it will be taken in this paper to investigate the reliability of the motor system of pure electric vans. The remaining parts of the paper are organized as below:

In Section 2, the motor system of pure electric vans will be briefly introduced so as the reader can have a basic understanding of it. In Section 3, the fault tree of the drive motor and motor controller will be developed and following which the mathematical methods for predicting the failure rates of basic events will be developed. To ease understanding, a case study is conducted in Section 4, in which the failure rate, reliability of the subassemblies in the motor system of the pure electric vans will be calculated and analyzed. The paper will be finally concluded in Section 5.

II. THE MOTOR SYSTEM IN PURE ELECTRIC VANS

As shown in Fig.1, the motor system of pure electric vans is a gearless system. It is simply composed of a drive motor and an associated motor controller. The drive motor will be used to drive the wheels directly via rear axle. The motor controller is used to control the torque, speed and rotation direction of drive motor according to the vehicle driving demand. Fig.1, the black and red dot lines are the Control Area Network (CAN) lines, it connecting the motor controller, Vehicle Control Unit (VCU) and the units that are designed to implement different control functions.

From Fig.1, the drive motor is the core component that is used to convert electrical energy into mechanical energy [18]. In order to ease understanding, the structure of the drive motor is shown in Fig.2.

As shown in Fig.2, the drive motor comprises a shell, stator, rotor, bearing, and position sensor. As soon as electric power is applied to the stator, a rotating magnetic field will be generated. Then, the rotor will be driven to rotate in the magnetic

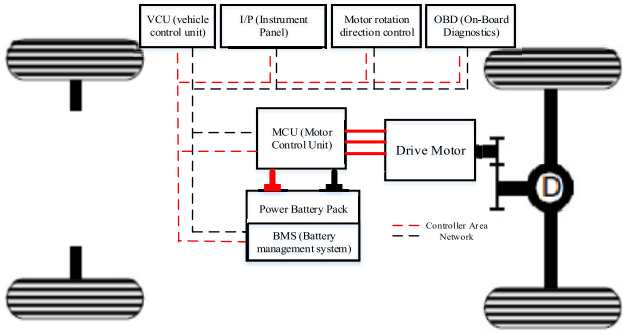

FIGURE 1. Schematic diagram of the motor system in pure electric vans.

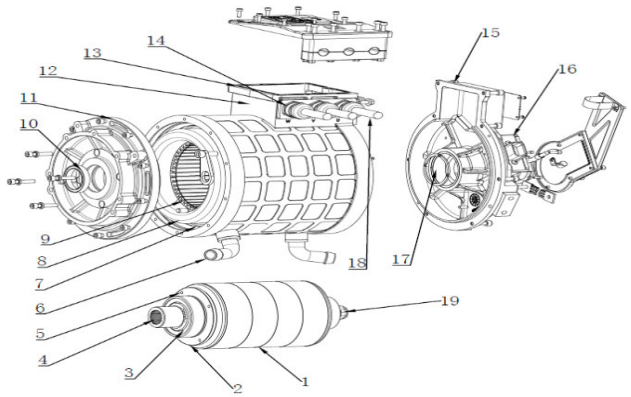

FIGURE 2. The structure of the drive motor in pure electric vans. 1 - rotor, 2 - rotor end cover, 3 - bearing, 4 - spline, 5 - fastening screw of rotor balance end cap, 6 - inlet of cooling water, 7 - jacket of cooling water, 8 - stator winding, 9 - core of stator, 10 - sealing rings of bearing, 11 - end cap fastening screw, 12 - junction box, 13 - seal ring, 14 - cable fixed head, 15 - fastening screw of rear end cap, 16 - position sensor, 17 - grease seal, 18 - three-phase lines, 19 - position sensor.

field due to the electromagnetic induction effect. Simultaneously, the relative position of the stator and rotor will be measured by the position sensor. Then the measured position will be input into the motor controller to ensure desired three-phase voltages are output from the motor controller. During the operation of the motor system, the temperature of the drive motor is detected by the temperature sensor (such as PT1000 shown in Table 6) in real-time. When the sensor fails, its resistance value will far exceed normal value and even will be recorded as infinity. In this case, the automatic detection program or system protection program of the motor controller will assume that the drive motor has been overheated, thereby shutting down the system automatically.

From Fig.3, it is seen that the motor controller is mainly composed of outer casing, thin-film capacitor, copper row, Insulated Gate Bipolar Translator (IGBT), driver module, control module, active discharging module, communication module, sealing ring, and cooling water jacket. Among them, the module refers to the equipped printed circuit board, which consists of connections, components, and board. For example, the control module consists of a control chip, resistances, capacitances, connections, and wire board. In the operation, an IGBT gate control signal will be output from the control

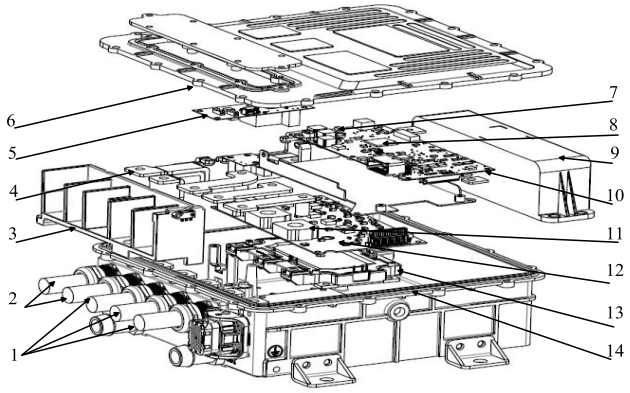

FIGURE 3. Schematic diagram of the motor controller. 1 - phase lines, 2 - power line, 3 – wiring slot, 4 - copper row, 5 - discharging module, 6 – housing shell, 7 - communication module, 8 - master chip, 9 - thin-film capacitor, 10 - control module, 11 - current transducer, 12 - driver module, 13 - IGBT, 14 - seal ring of shell.

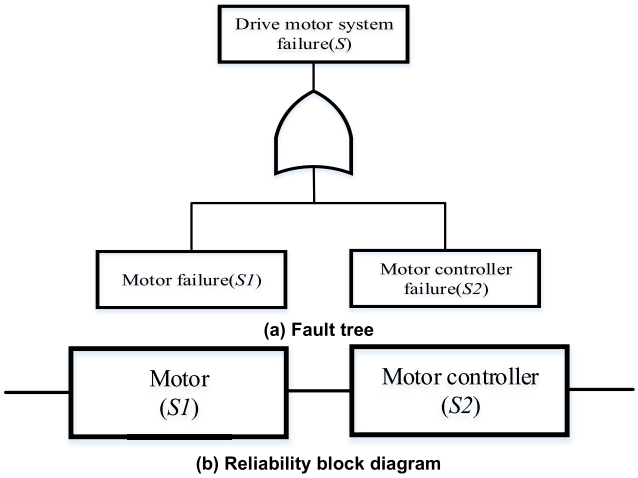

FIGURE 4. Fault tree and reliability block diagram of the motor system.

chip based on the position signal measured by the position sensor.

III. RELIABILITY STUDY OF MOTOR SYSTEM

Since fault tree analysis has been successfully applied to investigate the reliability of numerous systems [20], it will be taken to investigate the reliability of the motor system. Since the motor system is composed of a drive motor and motor controller, its fault tree model and reliability block diagram is shown in Fig.4. Accordingly, the reliability study in this section will comprise two parts. The first part is for investigating the reliability of the drive motor, and the second is for investigating the reliability of the motor controller.

A. RELIABILITY STUDY OF DRIVE MOTOR

As mentioned earlier, the drive motor is composed of bearings, rotor, stator, sensors, and other associated components. Its safety and efficiency can be affected once a fault occurs in any of these components. The survey has shown that the failures of oil seal, bearing, stators, and rotor winding account

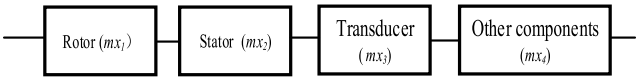

FIGURE 5. Reliability block diagram of the drive motor.

TABLE 1. Failure events of drive motor components.

Intermediate event	Code	Failure rate	Basic event	Code	Failure rate
Rotor failure	*gm1*	λ_{gm1}	Failure of rotor armature winding	*em1*	λ_{m1}
			Failure of rotor shaft	*em2*	λ_{m2}
Stator failure	*gm2*	λ_{gm2}	Failure of stator winding	*em3*	λ_{m3}
			Failure of stator core	*em4*	λ_{m4}
Transducer failure	*gm3*	λ_{gm3}	Failure of temperature sensor	*em5*	λ_{m5}
			Failure of position sensor	*em6*	λ_{m6}
Failure of other motor components	*gm4*	λ_{gm4}	Failure of spline	*em7*	λ_{m7}
			Failure of bearing oil seal	*em8*	λ_{m8}
			Failure of fastening screw	*em9*	λ_{m9}
			Failure of bearing	*em10*	λ_{m10}

for more than 80% of the total number of failures of the drive motor [21], herein the reliability study of the drive motor will be focused on the study of these vulnerable components which show high failure rate. Based on this understanding, the reliability block diagram of the drive motor is developed. It is shown in Fig.5.

For a reliability model shown in Fig.5, its reliability can be evaluated using the following equation.

$$\mathrm{R}_m(S_1) = P\,(mx_1)\,P\,(mx_2)\ldots P\,(mx_4) = \prod_{i=1}^{4} P(mx_i) \tag{1}$$

where $P(mx_i)$ refers to the reliability probability function of the i-th component in Fig.5.

In order to investigate the reliability of the components in the drive motor, the fault tree of the drive motor is developed, see Fig.6. In the figure, the top event *S1* is 'drive motor failure', and the basic events from *em1* to *em10* are the failure events of drive motor components. In this model, *gm1* to *gm4* are intermediate events (or logic gate events), which are the logical combination of the relevant basic events. All these events are explained in Table 1.

From Fig.6, it is found that the reliability of the drive motor relies on the reliability of bearing, motor rotor, motor stator, transducers, and other associated components. In order to understand the reliability of the drive motor, it is essential to evaluate the failure rates of these components. As long as the failure rates of these components and their corresponding reliability probability functions are obtained, the reliability of the drive motor can be readily assessed. According to the

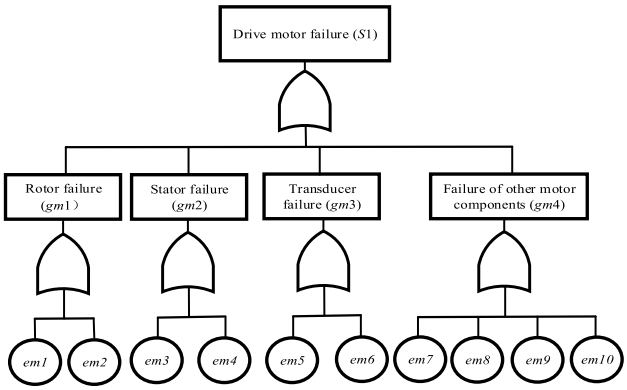

FIGURE 6. Fault tree of the drive motor.

handbook of the US Navy's mechanical equipment reliability prediction program [22], the failure rate of the basic events in Fig.6 can be estimated by

$$\begin{cases} \lambda_{1,3} = \lambda_{WI,B} C_{V1} C_{T1} C_{alt} \\ \lambda_2 = \lambda_{SH,B} C_{f2} C_{T2} C_{DY} C_{SC} \\ \lambda_4 = \lambda_{M,B} C_M \\ \lambda_5 = \lambda_{TD,B} + \lambda_{S5} + \lambda_{T5} + \lambda_{p5} + \lambda_{X6} \\ \lambda_6 = \lambda_{TD,B} + \lambda_{S6} + \lambda_{T6} + \lambda_{p6} + \lambda_{X6} \\ \lambda_7 = \lambda_{G,B} C_{GS} C_{GP} C_{GA} C_{GL} C_{GT} C_{GV} \\ \lambda_8 = \lambda_{SE,B} C_Q C_H C_{F8} C_{V8} C_{T8} C_N C_{PV} \\ \lambda_9 = \lambda_{F,B} C_{SZ} C_L C_{T9} C_I C_{SC9} C_K \\ \lambda_{10} = \lambda_{BE,B} C_{V10} C_{CW} C_{T10} C_{SF} \\ \lambda_{BE,B} = 2 \times 10^5 / \left(L_s / L_A\right)^y \end{cases} \tag{2}$$

All parameters in these equations are explained in Table 2 and the failure rate unit of each component is FPMH (failures per million hours).

From (2), it is seen that the failure rate of the components is dependent on their working environments, loads, and many other factors. Take the failure of the bearing as an example, its basic failure rate is

$$\lambda_{BE,B} = 2 \times 10^5 / L_{10} \tag{3}$$

where, $L_{10} = (L_s/L_A)^y$, L_s is basic dynamic load, L_A is equivalent radial load, and Y is a bearing life constant (Y = 3.0 for ball bearings, and 3.3 for roller bearings), and L_{10} can be also converted to hours by using the equation

$$L_{10h} = \frac{10^6}{60n} L_{10} \tag{4}$$

where, L_{10h} is the bearing life with operating hours, n is the rotational speed in the unit of revolution per minute.

From the Fig.6, the reliability of the rotor relies on the reliability of its winding and shaft. Therefore, the failure rate of the rotor is the sum of the failure rates of its winding and shaft, i.e.

$$\lambda_{gm1} = \lambda_{m1} + \lambda_{m2} \tag{5}$$

TABLE 2. Parameters in equation (2).

Symbol	Meaning	Symbol	Meaning	Symbol	Meaning
$\lambda_{WI,B}$	Base failure rate of drive motor windings	λ_{X5}	Failure rate of the temperature transmission other components	C_{PV}	Multiplying factor of pressure-velocity coefficient
C_{vI}	Multiplying factor of electrical source voltage variations	λ_{X6}	Failure rate of the position transmission other components	$\lambda_{F,B}$	Base failure rate of fasteners,
C_{TI}	Multiplying factor for drive motor windings	$\lambda_{G,B}$	Base failure rate of spline gears	C_{SZ}	Multiplying factor of size deviation
C_{alt}	Multiplying factor of operation at extreme elevation	C_{GT}	Multiplying factor considering the operation temperature	C_L	Multiplying factor of different loading application
$\lambda_{SH,B}$	Base failure rate of shaft	C_{GS}	Multiplying factor considering speed deviation	C_{T9}	Elevated temperature multiplying factor
C_{f2}	Shaft surface finish multiplying factor	C_{GP}	Multiplying factor considering actual spline gear loading	C_I	Multiplying factor of in-service cyclic shock loading
C_{dy}	Shaft displacement multiplying factor	C_{GA}	Multiplying factor considering misalignment	C_{sc9}	Surface coatings multiplying factor
C_{sc}	Stress Concentration factor for shaft grooves or keyway	C_{GL}	Multiplying factor considering lubrication deviation	C_k	Stress concentration multiplying factor for fastener threads
$\lambda_{M,B}$	Base failure rate of iron core	C_{GV}	Multiplying factor considering the AGMA service factor	$\lambda_{BE,B}$	Base failure rate of bearing
C_M	Iron core failure coefficient	$\lambda_{SE,B}$	Base failure rate of bearing grease seal	C_{v10}	Bearing lubricant synthesis coefficient
$\lambda_{TD,B}$	Base failure rate of sensor	C_Q	Multiplying factor of allowable leakage	C_{cw}	Bearing lubrication water-containing coefficient
λ_{S5}	Temperature transmitter failure rate	C_H	Multiplying factor of contact stress and seal hardness	C_{t10}	Working temperature comprehensive influence
λ_{S6}	Position transmitter failure rate	C_{F8}	Multiplying factor of seal surface finish	C_{sf}	Bearing operation and maintenance comprehensive
λ_{T5}	Failure rate of temperature transmission line	C_{V8}	Multiplying factor of fluid viscosity	Ls/L_A	Bearing load ratio
λ_{T6}	Failure rate of position transmission line	C_{T8}	Multiplying factor of seal face temperature	Y	Bearing life constant
λ_{P6}	Failure rate of the position transmission power source	C_N	Seal multiplying factor of contaminants		

Likewise, the failure rate of the stator, transducers and the other components in the drive motor can be respectively expressed as

$$\begin{cases} \lambda_{gm2} = \lambda_{m3} + \lambda_{m4} \\ \lambda_{gm3} = \lambda_{m5} + \lambda_{m6} \\ \lambda_{gm4} = \lambda_{m7} + \lambda_{m8} + \lambda_{m9} + \lambda_{m10} \end{cases} \tag{6}$$

The physical means of all variables in (5) and (6) can be found in Table 1.

B. RELIABILITY STUDY OF MOTOR CONTROLLER

As shown in Fig.3, the motor controller is composed of power electronic components and a housing shell. Due to the housing shell is reliable and has little chance to affect the reliability of the motor controller, it will not be considered in the following study. The motor controller consists of bus-bar capacitors, control module, driver module, discharging module, communication module, and IGBT. Since a fault occurring in any of these components can lead to the failure of the motor controller, the reliability block diagram of the motor controller can be described by using the diagram in Fig.7.

Based on Fig.7, the reliability of the motor controller can be predicted by [27]

$$\mathrm{R}_c(S_2) = P\left(cx_1\right) P\left(cx_2\right) \ldots P\left(cx_5\right) = \prod_{i=1}^{5} P(cx_i) \tag{7}$$

where $P(cx_i)$ indicates the reliability probability function of the i-th component in Fig.7.

Define the failure of the motor controller as the top event ($S2$) and the failures of these components as the basic events *ec1* to *ec14*, the fault tree of the motor controller can be constructed. It is shown in Fig.8. Where, the intermediate events are *gc1* to *gc4,* which are the logical combination of the relevant basic events. All these events are explained in Table 3.

Herein, it is worth noting that the capacitor mentioned in Table 3 is used to balance the power during the change of power frequency and the power output from the rectifier. On the one hand, it will absorb the energy produced by the drive motor when power switching devices are switched off in the scenario of an urgent stop. It will provide instantaneous

TABLE 3. Failure events of motor controller components.

Intermediate event	Code	Failure rate	Basic event	Code	Failure rate
Failure of control module	gc1	λ_{gc1}	PCB failure of control module	ec1	λ_{c1}
			SMCs failure of control module	ec2	λ_{c2}
			Master chip failure of control module	ec3	λ_{c3}
Failure of driver module	gc2	λ_{gc2}	PCB failure of driver module	ec4	λ_{c4}
			SMCs failure of driver module	ec5	λ_{c5}
			Optocoupler failure	ec6	λ_{c6}
Failure of discharging module	gc3	λ_{gc3}	PCB failure of discharging module	ec7	λ_{c7}
			SMCs failure of discharging module	ec8	λ_{c8}
			MOSFET failure	ec9	λ_{c9}
Failure of communication module	gc4	λ_{gc4}	PCB failure of communication module	ec10	λ_{c10}
			SMC failure of communication module	ec11	λ_{c11}
			Communication chip failure	ec12	λ_{c12}
Failure of other controller components	gc5	λ_{gc5}	Busbar capacitor failure	ec13	λ_{c13}
			IGBT failure	ec14	λ_{c14}

Note: SMC – surface-mounted component, PCB – Printed circuit board.

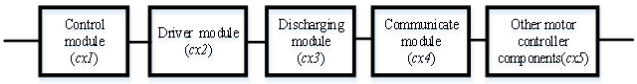

FIGURE 7. Reliability block diagram of the motor controller.

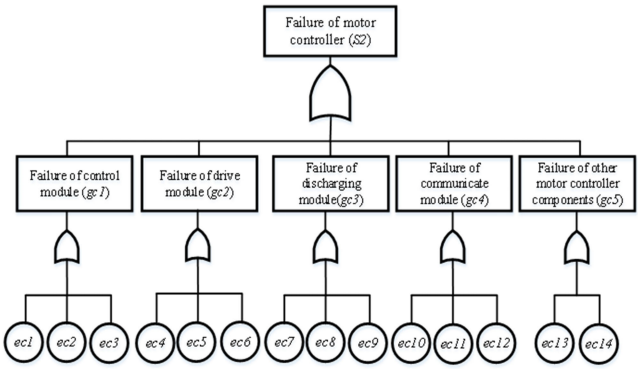

FIGURE 8. Fault tree of motor controller.

peak power as required so as the inverter can be well protected during the sudden change of power. At present, the capacitors used in the motor controllers of pure electric vans are film capacitors. Its failure rate can be evaluated by using equation [24]

$$\lambda_{c13} = 0.1\left(\left[\frac{\sum_{i=1}^{y}\left(\pi_{t_{c13}}\right)_i \tau_i}{\tau_{on}+\tau_{off}}\right] + 1.4\times10^{-3} \times \left[\sum_{i=1}^{j}(\pi_n)_i\,(\Delta T_i)^{0.68}\right]\right)\times10^{-9} \quad (8)$$

where $(\pi_t)_i$ is the i-th temperature factor related to the i-th junction temperature of the capacitor mission profile; $\left(\pi_{t_{c13}}\right) = e^{2900\left(\frac{1}{303}-\frac{1}{273+t_{A_{c13}}}\right)}$ is a factor reflecting the influence of ambient temperature $t_{A_{c13}}$; τ_{on} is the total working time ratio of the capacitor; τ_{off} is time ration for the capacitor being in storage (or dormant) mode; $(\pi_n)_i$ is the i-th influence factor related to the annual cycles number of thermal variation with the amplitude ΔT_i; ΔT_i refers to the i-th thermal amplitude variation of the mission profile.

The control module in Table 3 comprises a master chip, a printed circuit board (PCB), and some surface-mounted components (SMCs). The SMCs include inductors, resistors, capacitors, transformers, integrated chips, diodes, etc. So, the reliability of the control module relies on the reliability of the master chip, PCB and SMCs. The failure rate of these components can be evaluated by [23], [24], [26]

$$\begin{cases} \lambda_{c1} = 5\times10^{-3}\pi_{t_{c1}}\pi_c\left[N_t\sqrt{1+\frac{N_t}{S}}+N_p\frac{1+0.1\sqrt{S}}{3}\pi_L\right] \\ \qquad \times\left(1+3\times10^{-3}\left[\sum_{i=1}^{j}(\pi_n)\,(\Delta T_i)^{0.68}\right]\right)\times10^{-9} \\ \lambda_{c2} = \sum\lambda_s\times10^{-9} \\ \qquad +\left(\sum\lambda_f+\left(1+3\times10^{-3}\right)\left[\sum_{i=1}^{j}(\pi_n)i(\Delta T_i)^{0.68}\right]\right) \\ \qquad \times10^{-9}\times\sum\lambda_d \\ \lambda_{ci} = (C_{i1}\pi_{it}+C_{i2}\pi_{iE})\,\pi_{iQ} \\ \lambda_{cc} = \lambda_{cb}\pi_{cE}\pi_{cQ}\pi_{cT}\pi_{cS}\pi_{cch} \\ \lambda_{cg} = \lambda_{gb}\pi_{gE}\pi_{gQ}\pi_{gT} \\ \lambda_{cr} = \lambda_{rb}\pi_{rE}\pi_{rQ}\pi_{rR} \\ \lambda_{cm} = \lambda_{mb}\pi_{mE}\pi_{mQ}\pi_{mr}\pi_{mA}\pi_{mC}\pi_{mK} \end{cases} \quad (9)$$

where $\pi_{t_{c1}} = e^{1740\left(\frac{1}{303}-\frac{1}{273+t_{A_{c1}}}\right)}$ is a factor indicating the influence of ambient temperature $t_{A_{c1}}$; π_C indicates the influence of the number of layers; N_t is the total number of holes; S is the surface area of the board; N_P is the number of tracks. Its default value is $N_P = \frac{\sum N_s+\sum N_f}{2}$, in which N_s is the number of lines that connect to every component, N_f is the number of components that connect to every hole; π_L is the coefficient of line track width, ΔT_i is the variation of temperature; λ_d is the interconnection failure rate. Other parameters in (8) are further explained in Table 4.

Then, the failure rate of the control module in the motor controller can be evaluated by [27].

$$\lambda_{gc1} = \lambda_{c1}+\lambda_{c2}+\lambda_{c3} \quad (10)$$

TABLE 4. Other parameters in equation (8).

Symbol	Meaning	Symbol	Meaning	Symbol	Meaning
λ_S	SMCs failure rate	π_{cQ}	Capacitance quality factor	π_{rE}	Resistance environment factor
λ_f	Failure rate of THCs	π_{cT}	Capacitance temperature factor	π_{rQ}	Resistance quality factor
λ_{Ci}	Integrated chip failure rate	π_{cS}	Capacitance electric stress coefficient	π_{rR}	Resistance value coefficient
C_{il}	Integrated chip complexity failure rate	π_{cch}	Capacitance surface mount factor	λ_{Cm}	MOSFET failure rate
π_{iT}	Integrated chip temperature stress coefficient	λ_{cg}	Inductance failure rate	λ_{mb}	Basic failure rate of MOSFET
π_{iE}	Integrated chip environment factor	λ_{gb}	Base failure rate of inductance	π_{mE}	MOSFET environment factor
C_{i2}	Encapsulation complexity failure rate	π_{gE}	Inductance environment factor	π_{mQ}	MOSFET quality factor
π_{iQ}	Integrated chip quality factor	π_{gQ}	Inductance quality factor	π_{mA}	MOSFET application factor
λ_{cc}	Ceramic capacitance failure rate	π_{gT}	Inductance temperature factor	π_{mC}	MOSFET construction coefficient
λ_{cb}	Basic failure rate of capacitance	λ_{cr}	Resistance failure rate	π_{mr}	MOSFET rated power factor
π_{cE}	Capacitance environment factor	λ_{rb}	Base failure rate of resistance	π_{mK}	MOSFET species coefficient

Note: THCs – through hole components

TABLE 5. Performance parameters of the motor system being investigated.

Item	Parameters	Item	Parameters
Motor type	Asynchronous induction	Controller capacity	75 KVA
Maximum output power	35/65 kW	Maximum working voltage	460 V
Maximum speed	3000/8500 rpm	Controller output frequency range	0~600 Hz
Peak torque	260Nm	Peak point current	320 A
Nominal voltage	DC307 V	Controller nominal voltage	DC307 V
Motor cooling mode	Water-cooling	Controller cooling mode	Water-cooling

As the hardware components of the driver module, discharging module, and communication module of the motor controller are similar to the control module, their failure rate can be evaluated in the same way, i.e.

$$\begin{cases} \lambda_{gc2} = \lambda_{c4} + \lambda_{c5} + \lambda_{c6} \\ \lambda_{gc3} = \lambda_{c7} + \lambda_{c8} + \lambda_{c9} \\ \lambda_{gc4} = \lambda_{c10} + \lambda_{c11} + \lambda_{c12} \\ \lambda_{gc5} = \lambda_{c13} + \lambda_{c14} \end{cases} \tag{11}$$

where $\lambda_{gc2} - \lambda_{gc5}$ refer to the failure rate of the driver module, discharging module, communication module and the other components in the motor controller, respectively (show in Table.3).

TABLE 6. Parts of the drive motor.

Part	Model/Specification	Quantity
Hexagonal socket head cap screw	M6×20-12.9-NiZn/M6×12-NiZn	28 Sets
Oil seal	TC 40×52×8 Fluorine rubber	2 Sets
Elastic ring for shaft	GB/T 894.1 40	2 Sets
Deep groove ball bearing	6206-2Z/C3, WT	2 Sets
O-rings	204×2.65-A-S-GB/T 3452.1	2 Sets
Position sensor	TS2225N1994E102	1 Sets
Temperature sensor	PT1000	2 Sets

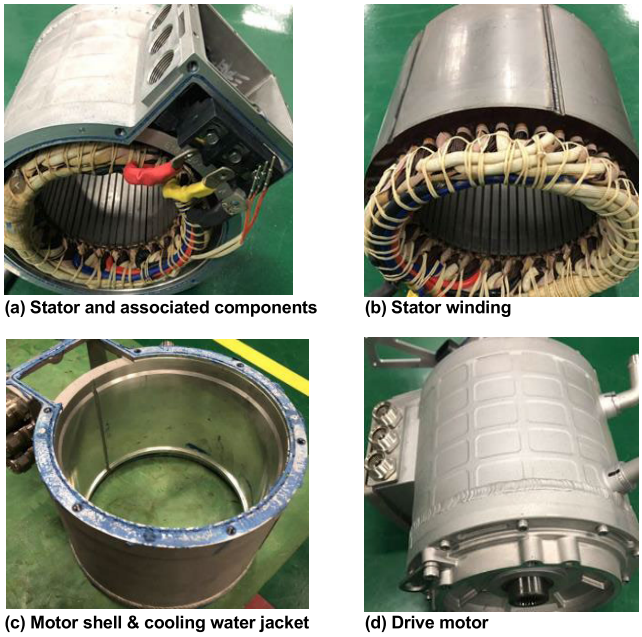

(a) Stator and associated components (b) Stator winding

(c) Motor shell & cooling water jacket (d) Drive motor

FIGURE 9. The drive motor being investigated.

IV. CASE STUDY

A case study is conducted in this section in order to quantitatively assess the reliability of the motor system in pure electric vans by using the mathematical methods described in section 3. The performance parameters of the motor system are listed in Table 5.

A. EVALUATION OF FAILURE RATES OF DRIVE MOTOR PARTS

To ease understanding, the drive motor of interest is shown in Fig.9 and its parts are listed in Table 6.

As mentioned earlier, the failure of the drive motor is mainly caused by the faults developed in bearing, rotor,

TABLE 7. Parameters for calculating the failure rates of drive motor components.

Name	symbol	units	value	Name	symbol	units	value
Base failure rate of motor windings	$\lambda_{WI,B}$	*FPMH*	0.50	Multiplying factor considering misalignment	C_{GA}	*NA*	2.80
Multiplying factor of electrical source voltage variations	C_{vl}	*NA*	1.10	Multiplying factor considering lubrication deviation	C_{GL}	*NA*	0.86
Multiplying factor of operation at extreme elevation	C_{alt}	*NA*	1.80	Multiplying factor considering the service factor	C_{GV}	*NA*	1.25
Multiplying factor for motor windings	C_{Tl}	*NA*	0.28	Base failure rate of dynamic seal	$\lambda_{SE,B}$	*FPMH*	2.40
Base failure rate of bearing	$\lambda_{SH,B}$	*FPMH*	0.02	Multiplying factor of seal surface finish	C_{F8}	*NA*	1.30
Shaft surface finish multiplying factor	C_{f2}	*NA*	1.00	Multiplying factor of fluid viscosity	C_{vi}	*NA*	0.14
Shaft displacement multiplying factor	C_{dy}	*NA*	0.78	Multiplying factor of seal face temperature	C_{T8}	*NA*	1.89
Stress concentration factor for shaft grooves or keyway	C_{sc}	*NA*	1.45	Seal multiplying factor of contaminants	C_N	*NA*	0.79
Base failure rate of iron core	$\lambda_{M,B}$	*FPMH*	0.003	Seal pressure-velocity coefficient	C_{pv}	*NA*	0.76
Multiplying factor for iron core	C_M	*NA*	0.10	Base failure rate of fasteners	$\lambda_{F,B}$	*FPMH*	1.00
Base failure rate of temperature sensor	$\lambda_{TD,B}$	*FPMH*	1.00	Multiplying factor of size deviation	C_{SZ}	*FPMH*	1.00
Temperature transmitter failure rate	λ_{S5}	*FPMH*	0.39	Multiplying factor of different loading application	C_L	*NA*	1.00
Position transmitter failure rate	λ_{S6}	*FPMH*	0.30	Elevated temperature multiplying factor	C_{T9}	*NA*	1.00
Failure rate of temperature transmission line	λ_{T5}	*FPMH*	0.01	Multiplying factor considering the severity of in-service cyclic shock loading	C_I	*NA*	1.25
Failure rate of position transmission line	λ_{T6}	*FPMH*	0.03	Surface coatings multiplying factor	C_{sc9}	*NA*	1.16
Failure rate of the position transmission power source	λ_{P6}	*FPMH*	0.04	Stress concentration multiplying factor for fastener threads	C_k	*NA*	3.00
Failure rate of the temperature transmission other components	λ_{X5}	*FPMH*	0.01	Bearing lubricant synthesis coefficient	C_{v10}	*NA*	1.1
Failure rate of the position transmission other components	λ_{X6}	*FPMH*	0.02	Bearing lubrication water-containing coefficient	C_{cw}	*NA*	3.25
Base failure rate of spline gears	$\lambda_{G,B}$	*FPMH*	1.00	Bearing operation and maintenance comprehensive coefficient	C_{sf}	*NA*	1.10
Multiplying factor considering speed deviation	C_{GS}	*NA*	1.42	Working temperature comprehensive coefficient	C_{t10}	*NA*	1.00
Multiplying factor considering actual spline gear loading	C_{GP}	*NA*	0.12	Bearing life constant	Y	*NA*	3
Multiplying factor considering the operation temperature	C_{GT}	*NA*	0.21	Bearing load ratio	Ls/L_A	*NA*	2
Multiplying factor of allowable leakage	C_Q	*NA*	0.90	Bearing life	L_{10}	$rpm*10^{-6}$	8
Multiplying factor of contact stress and seal hardness	C_H	*NA*	1.00	Motor speed	n	*rpm*	5000

Note: FPMH – failures per million hours; NA – Not Applicable

stator, and other associated components. Therefore, according to the Handbook of Reliability Prediction Procedures for Mechanical Equipment NSWC-09 [22] and Chinese electric vehicle technical requirements standards [25], [26], all parameters used for calculating the failure rate of these drive motor components can be readily obtained. They are listed in Table 7.

Then, calculate the failure rate of every component in the fault tree model of the drive motor by substituting these parameters into (2)-(6). The obtained calculation results

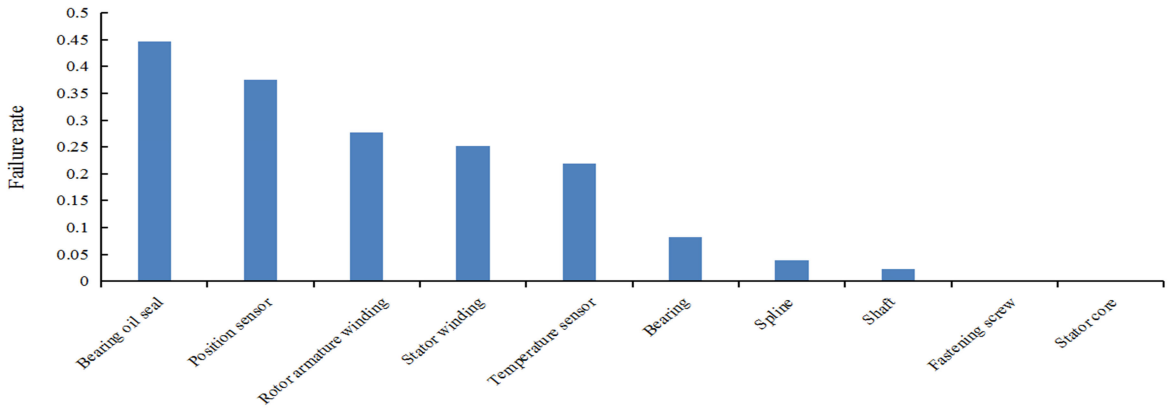

FIGURE 10. Calculation results of the failure rate of drive motor components.

TABLE 8. Calculation results of the failure rates of drive motor components.

Codes	Failure rate /FPMH	Codes	Failure rate /FPMH	Codes	Failure rate /FPMH
λ_{gm1}	0.2998	λ_{m1}	0.2772	λ_{m6}	0.0375
λ_{gm2}	0.2523	λ_{m2}	0.0226	λ_{m7}	0.0385
λ_{gm3}	0.2580	λ_{m3}	0.2520	λ_{m8}	0.4465
λ_{gm4}	0.5683	λ_{m4}	0.0003	λ_{m9}	0.0003
		λ_{m5}	0.2195	λ_{m10}	0.0830

TABLE 9. Physical means of the parameters.

Symbol	Meaning	Symbol	Meaning	Symbol	Meaning
λ_{tci}	Total failure rate of resistance	n_i	Number of resistances	λ_{ci}	Failure rate of a single resistance
λ_{tcc}	Total failure rate of capacitance	n_c	Number of capacitances	λ_{cc}	Failure rate of a single capacitance
λ_{tcg}	Total failure rate of inductance	n_g	Number of inductances	λ_{cg}	Failure rate of a single inductance
λ_{tcm}	Total failure rate of MOSFET	n_m	Number of MOSFET	λ_{cm}	Failure rate of a single MOSFET

are listed in Table 8. In order to facilitate interpretation, the results are further illustrated in Fig.10.

From the calculation results shown in Table 8 and Fig.10, it is found that the oil seal of the bearing is the most vulnerable part in the drive motor, followed by the position sensor and rotor/stator windings. The temperature sensor is also prone to develop failure in operation. By contrast, the motor bearing, the spline, and the shaft are relatively more reliable. The fastening screw and stator core are the most reliable components in the drive motor, they are nearly free of fault.

B. EVALUATION OF FAILURE RATES OF MOTOR CONTROLLER PARTS

The failure of the motor controller is primarily caused by the faults occurring in the busbar capacitor, control module, driver module, discharging module, communication module, and IGBT. All these parts are illustrated in Fig.11.

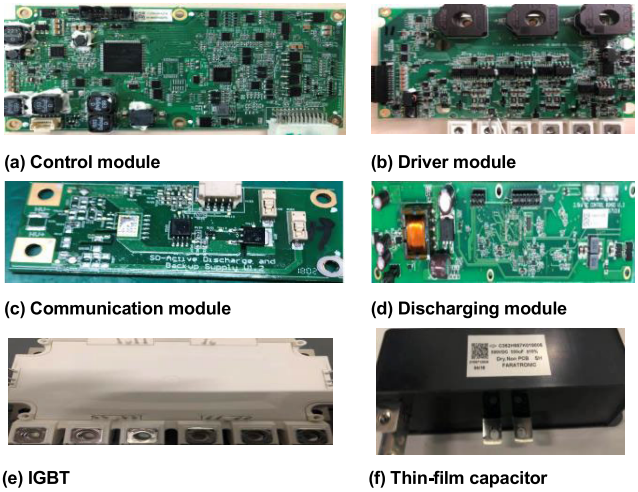

(a) Control module (b) Driver module

(c) Communication module (d) Discharging module

(e) IGBT (f) Thin-film capacitor

FIGURE 11. Parts of the motor controller.

From the design documents and Bill of Material (BOM) provided by the motor systems manufacturer, it is known that the model of busbar capacitor is C362H557K19802 and the model of IGBT is FS400R07A3E3. As there are many SMCs on the PCB and they have a variety of specifications, it is not realistic to evaluate the failure rate of every component one by one. To deal with this issue, the SMCs in BOM list are classified first according to their types, such as resistance, inductance, capacitance, etc. Then, the failure rate of the same type of SMCs is calculated by using the following counting method.

$$\begin{cases} \lambda_{tci} = n_i \lambda_{ci} \\ \lambda_{tcc} = n_c \lambda_{cc} \\ \lambda_{tcg} = n_g \lambda_{cg} \\ \lambda_{tcr} = n_r \lambda_{cr} \\ \lambda_{tcm} = n_m \lambda_{cm} \end{cases} \tag{12}$$

All variables in the above equations are explained in Table 9.

TABLE 10. Parameters used for calculating the failure rates of SMCs.

Name	codes	Value/*FPMH*	Name	codes	Value/*FPMH*
PCB layer coefficient of control module (4 layers)	π_{cc1}	1.4	Number of SMCs on control module	N_{sc1}	609
PCB layer coefficient of driver module (4 layers)	π_{cc2}	1.4	Number of SMCs on driver module	N_{sc2}	463
PCB layer coefficient of discharging module (2 layers)	π_{cc3}	1	Number of SMCs on discharging module	N_{sc3}	14
PCB layer coefficient of communication module (2 layers)	π_{cc4}	1	Number of SMCs on communication module	N_{sc4}	32
Track width factor of PCB in control module (0.23mm)	π_{Lc1}	3	Number of THCs of control module	N_{fc1}	0
Track width factor of PCB in driver module (0.6mm)	π_{Lc2}	1	Number of THCs of driver module	N_{fc2}	0
Track width factor of PCB in discharging module (0.6mm)	π_{Lc3}	1	Number of THCs of discharging module	N_{fc3}	2
Track width factor of PCB in communication module (0.35mm)	π_{Lc4}	2	Number of THCs on communication module	N_{fc4}	0
Tracks number of PCB in control module	N_{pc1}	720	Surface area of control module	S_{c1}	144
Tracks number of PCB in driver module	N_{pc2}	510	Surface area of driver module	S_{c2}	144
Tracks number of discharging module	N_{pc3}	20	Surface area of discharging module	S_{c2}	24
Tracks number of communication module	N_{pc4}	38	Surface area of communication module	S_{c3}	28

Note: THCs – through hole components

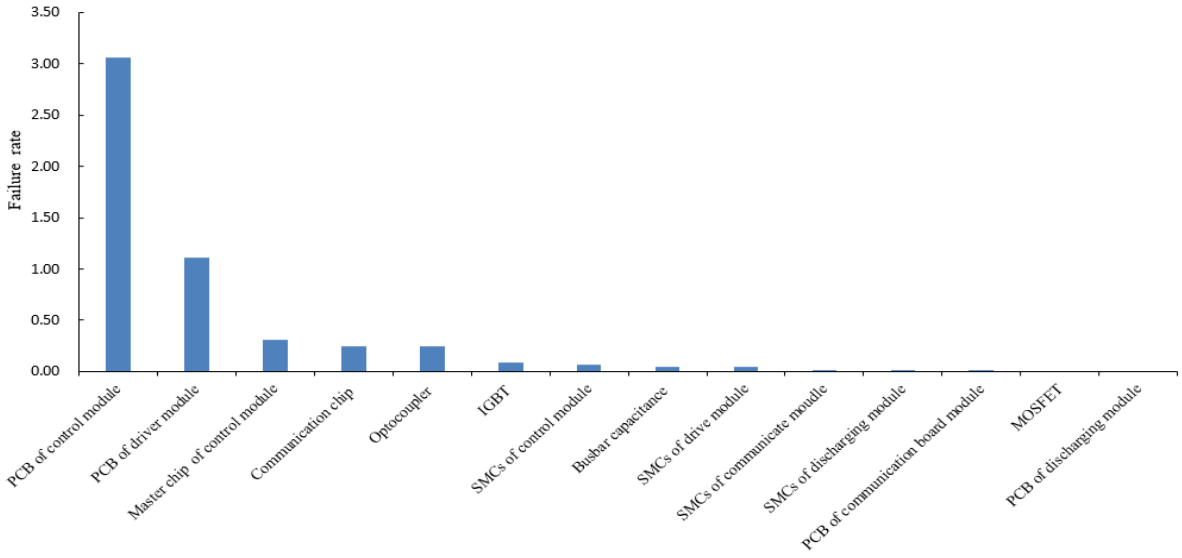

FIGURE 12. Calculation results of the failure rates of different motor controller parts.

According to IEC TR62308-2004, MIL-HDBH-217E and the technical standards for the Chinese electric vehicle industry [23], [24], [26], the failure rates of all SMCs are calculated. The parameters used for calculating the failure rate are listed in Table 10, and failure rate calculation results are listed in Table 11.

Based on the data listed in Table 11, the failure rate of motor controller parts is calculated by substituting these parameters into (8-12). The calculation results are listed in Table 12. In parallel, the calculation results are also illustrated in Fig.12 so as the reader can have an intuitive understanding of the reliability of the different parts of the motor controller.

From Fig.12, it is found that the PCB of the control module is the most vulnerable part in the motor controller (i.e. its failure rate is as high as 3.058), followed by the PCB of the drive board module (i.e. its failure rate is 1.116). The master chip and communication chip, as well as optocoupler,

TABLE 11. SMCs on boards and their failure rate calculation results.

Component	Type of Package	Number	Single device failure rate/*FPMH*
SMCs on the control module			
Ceramic capacitor	0603-C	265	0.00306
Diode	SOD/SOT	59	0.55440
Op-amp chip	TSSOP	14	1.26230
Inductance	MSS	23	0.07762
MOSFET	SOT/DPAK	18	0.59700
Resistance	0603-R	230	0.00018
Master chip	LQFP144	1	0.30950
SMCs on the driver module			
Ceramic capacitor	1206-C/0603-C	176	0.00306
Diode	SM/SOD	60	0.55440
Op-amp chip	TSSOP	3	1.26230
Inductance	MSS	23	0.07762
MOSFET	SOT	19	0.59700
Resistance	0603-R/2512/1206	173	0.00018
Optocoupler	SO8	3	0.08100
Transformer	CEER117	6	0.13100
SMCs on the discharging module			
Ceramic capacitor	0603-C	2	0.00306
MOSFET	SOT	2	0.59700
Resistance	0603-R	10	0.00018
Driver chip of MOSFET	DEIC420	2	0.00210
SMCs on the communication module			
Ceramic capacitor	0603-C	9	0.00306
Diode	SOD/SOT	5	0.55440
Communication chip	TSSOP	2	0.12600
Inductance	MSS	6	0.07762
Resistance	0603-R	10	0.00018

are also prone to develop a fault in operation. But they are relatively more reliable than the PCB of the control and driver module. Their failure rate varies in the range of 0.2-0.35. In comparison, the IGBT and SMCs, as well as the PCB of the communication module and discharging module, have little chance to develop a fault in operation as their failure rate is below 0.1.

TABLE 12. Failure rates of motor controller parts.

Codes	Failure rate /FPMH	Codes	Failure rate /FPMH	Codes	Failure rate /FPMH
λ_{gc1}	3.44	λ_{c3}	0.310	λ_{c10}	0.012
λ_{gc2}	1.402	λ_{c4}	1.116	λ_{c11}	0.019
λ_{gc3}	0.027	λ_{c5}	0.043	λ_{c12}	0.252
λ_{gc4}	0.283	λ_{c6}	0.243	λ_{c13}	0.051
λ_{gc5}	0.136	λ_{c7}	0.005	λ_{c14}	0.085
λ_{c1}	3.058	λ_{c8}	0.018		
λ_{c2}	0.072	λ_{c9}	0.004		

The comparison of Table 8 and Table 12 has shown that the overall reliability of the motor controller is lower than that of the drive motor. In the global view of the motor system, its control module is most vulnerable, the failure rate of which is as high as 3.44. The second is the driver module. Its failure rate is 1.402. The motor rotor, stator, transducers, and communication module have similar failure rates. They are 0.2998, 0.2523, 0.2580, and 0.2830, respectively. The understanding of such a figure is of great significance to the reliability design and maintenance of pure electric vans.

C. UNRELIABILITY INDEX

Although the calculation results presented above have indicated the reliability of individual components, the information provided by them remains the 'snapshots' of the reliability of the motor system. For this reason, the unreliability indices of the drive motor and motor controller as well as the entire motor system are evaluated based on the above calculation results in order to obtain a more comprehensive understanding of the reliability of the motor system. Herein, the unreliability indices of the drive motor and its controller are estimated with the aid of Eqns. (1) and (7). The equations for calculating the unreliability indices are

$$\begin{cases} F_m(t) = 1 - R_m(S_1) \\ F_c(t) = 1 - R_C(S_2) \\ F_{mc}(\mathrm{t}) = 1 - (1 - F_m(t))(1 - F_c(t)) \end{cases} \tag{13}$$

where F_m, F_c and F_{mc} refer to the unreliability indices of the drive motor, motor controller, and the whole motor system, respectively; R_m, R_c refer to the reliability indices of the drive motor, motor controller, respectively.

The corresponding estimation results when the service life of the motor system reaches respectively 10,000, 30,000, 50,000 and 70,000 hours are shown in Fig.13.

From Fig.13, it is clearly seen that

(1) the motor controller is much less reliable than the drive motor. This agrees very well with the research conclusion obtained from the failure rate calculation results in Section 4.2;

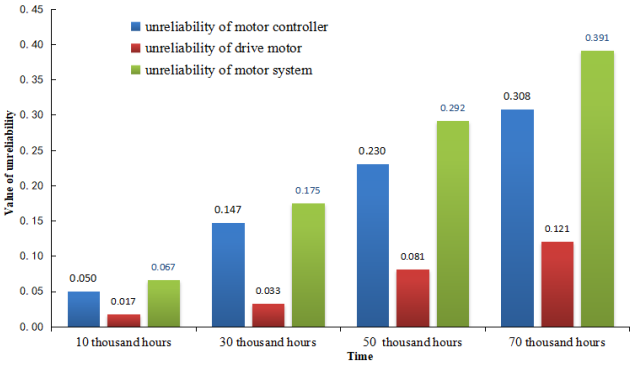

FIGURE 13. Calculation results of the unreliability index of the drive motor and motor controller.

(2) both drive motor and motor controller will become more and more unreliable with the increase of their service time, i.e. the longer the service time, the higher their unreliability indices will tend to be;
(3) the most important is that despite the service time, the calculation result of the unreliability index of the entire motor system is much higher than the corresponding value of the unreliability index of the drive motor. This suggests that the entire motor system, in fact, has less reliability than drive motor.

V. CONCLUSION

In order to provide a more reliable prediction to the entire motor system in pure electric vans, a detailed study of the reliability issues in both drive motor and motor controller are investigated in this paper by the approach of fault tree analysis. From the research reported above, the following conclusions can be drawn

- Due to aging, the reliability of both drive motor and motor controller will decrease gradually with the increase of their service time;
- Despite the service time, in the entire motor system, the motor controller is more unreliable than drive motor. For example, when the motor system continuously runs for 30,000 hours, the unreliability of drive motor is 0.033, but the unreliability of motor controller has reached as high as 0.147, which is about 4.5 times of the unreliability of the former;
- The control module is not only the most vulnerable part of the motor controller but also the most vulnerable part of the entire motor system. This is due to the application of a large number of electronic components (the total number of electronic devices in the control module is up to 610 PCS), and more electronic devices will lead to more connecting lines, thinner line widths and more through holes on the PCB, which will reduce the reliability of the control module;
- The reliability issues in the drive motor and motor controller should be investigated together when assessing the reliability of the motor system. Otherwise, an unreliable reliability prediction may be obtained. This is because the drive motor and motor controller are logically integrated and are always requested to work as one system in the EVs. The reliability of the entire motor system will be less estimated if only the reliability issues in the drive motor are considered in the assessment.

ACKNOWLEDGMENT

The authors gratefully acknowledge Prof. B. Pailthorpe and Dr. N. Bordes for useful discussions and consultations.

REFERENCES

[1] China Passenger Car Association. *Electric Vehicle Sales Analysis for the Global Market from 2018 to 2019*. Accessed: Feb. 30, 2019. [Online]. Available: http://www.cpcaauto.com/newslist.asp?types=csjd&id=9435
[2] F. P. Santos, P. Teixeira, and C. G. Soares, "Operation and maintenance of floating offshore wind turbines," in *Floating Offshore Wind Farms*. Cham, Switzerland: Springer, Mar. 2016, pp. 181–193, doi: 10.1007/978-3-319-27972-5_10.
[3] F. H. Gandoman, A. Ahmadi, P. V. D. Bossche, J. Van Mierlo, N. Omar, A. E. Nezhad, H. Mavalizadeh, and C. Mayet, "Status and future perspectives of reliability assessment for electric vehicles," *Rel. Eng. Syst. Saf.*, vol. 183, pp. 1–16, Mar. 2019, doi: 10.1016/j.ress.2018.11.013.
[4] I. Bolvashenkov, J. Kammermann, and H. G. Herzog, "Research on reliability and fault tolerance of multi-phase traction electric motors based on Markov models for multi-state systems," in *Proc. SPEEDAM*, Aug. 2016, pp. 1166–1171, doi: 10.1109/SPEEDAM.2016.7525928.
[5] M. S. Blanco, "The economics of wind energy," *Renew. Sustain. Energy*, vol. 13, pp. 387–401, Aug./Sep. 2009, doi: 10.1016/j.rser.2008.09.004.
[6] R. Yan, L. M. Jackson, and S. J. Dunnett, "Automated guided vehicle mission reliability modelling using a combined fault tree and Petri net approach," *Int. J. Adv. Manuf. Technol.*, vol. 92, no. 5, pp. 1825–1837, Mar. 2017, doi: 10.1007/s00170-017-0175-7.
[7] R. D. Yan, S. J. Dunnett, and L. M. Jackson, "Novel methodology for optimizing the design, operation and maintenance of a multi-AGV system," *Rel. Eng. Syst. Saf.*, vol. 178, pp. 130–139, Oct. 2018, doi: 10.1016/j.ress.2018.06.003.
[8] D. Wanner, "Faults and their influence on the dynamic behavior of electric vehicles," Ph.D. dissertation, Dept. Vehicle Eng., Roy. Inst. Technol. Vehicle Dyn., Teknikringen, Stockholm, Sweden, 2013.
[9] B. Wang, G. Tian, Y. Liang, and T. Qiang, "Reliability modeling and evaluation of electric vehicle motor by using fault tree and extended stochastic Petri nets," *J. Appl. Math.*, vol. 2014, pp. 1–9, Apr. 2014, doi: 10.1155/2014/638013.
[10] B. Wang, Y. Liang, C. Yang, and Z. Sang, "Reliability modeling and assessment of electric vehicle motor using fault tree and fuzzy Petri nets," *Int. J. Grid Distrib. Comput.*, vol. 9, no. 8, pp. 121–136, Aug. 2016, doi: 10.14257/ijgdc.2016.9.8.12.
[11] X.-H. Zhu, S.-M. Gui, and N. Shi, "Grey prediction model of motor reliability of electric vehicle," *Electr. Mach. Control*, vol. 16, no. 8, pp. 41–42, Aug. 2012.
[12] M. Khalilzadeh and A. Fereidunian, "A Markovian approach applied to reliability modeling of bidirectional DC-DC converters used in PHEVs and smart grids," *Iranian J. Elect. Electron. Eng.*, vol. 4, no. 12, pp. 13–301, Dec. 2016, doi: 10.22068/IJEEE.12.4.301.
[13] Y. Song and B. Wang, "Survey on reliability of power electronic systems," *IEEE Trans. Power Electron.*, vol. 28, no. 1, pp. 591–604, Jan. 2013, doi: 10.1109/tpel.2012.2192503.
[14] J. Kang, L. Sun, and C. G. Soares, "Fault tree analysis of floating offshore wind turbines," *Renew. Energy*, vol. 133, pp. 1455–1467, Apr. 2019, doi: 10.1016/j.renene.2018.08.097.
[15] T. P. KhanhNguyen, J. Beugin, and J. Marais, "Method for evaluating an extended fault tree to analyses the dependability of complex systems: Application to a satellite-based railway system," *Rel. Eng. Syst. Saf.*, vo133, pp. 300–313, Jan. 2014, doi: 10.1016/j.ress.2014.09.019.
[16] X. Zhang, L. Sun, H. Sun, Q. Guo, and X. Bai, "Floating offshore wind turbine reliability analysis based on system grading and dynamic FTA," *J. Wind Eng. Ind. Aerodyn.*, vol. 154, pp. 21–33, Jul. 2016, doi: 10.1016/j.jweia.2016.04.005.
[17] B. Hu and P. Seiler, "Pivotal decomposition for reliability analysis of fault tolerant control systems on unmanned aerial vehicles," *Rel. Eng. Syst. Saf.*, vol. 140, pp. 130–141, Aug. 2015, doi: 10.1016/j.ress.2015.04.005.

[18] M. Hernandez, M. Messagie, M. De Gennaro, and J. Van Mierlo, "Resource depletion in an electric vehicle powertrain using different LCA impact methods," *Resour., Conservation Recycling*, vol. 120, pp. 119–130, May 2017, doi: 10.1016/j.resconrec.2016.11.005.
[19] E. Dabla, C. Martin, F. Pérès, F. Andrianoelison, and M. Piton, "Contribution of Bayesian network to the prediction of reliability of IGBT module used in railway applications," in *Proc. 16th IFAC Symp. Inf. Control Problems Manuf.*, Bergamo, Italy, Jan. 2018, doi: 10.1016/j.ifacol.2018.08.265.
[20] S. Kabir, "An overview of fault tree analysis and its application in model-based dependability analysis," *Expert Syst. Appl.*, vol. 77, pp. 114–135, Jul. 2017, doi: 10.1016/j.eswa.2017.01.058.
[21] L. Wang, A. Liao, and Y. Ding, "Reliability evaluation of rolling bearings for traction motors of bogies based on proportional hazards model," *Meas. Control Technol.*, vol. 31, no. 1, pp. 14–19, Jan. 2018.
[22] *Handbook of Reliability Prediction Procedures for Mechanical Equipment*, Nav. Surf. Warfare Center Carderock Division, Potomac, MD, USA, 2009, pp. 14–29.
[23] *Military Handbook Reliability Prediction of Electronic Equipment MIL-HDBH-217E*, Dept. Defense Assistance Mil., Federal Agencies, Ind., Washington, DC, USA, 1990.
[24] *Reliability Date Handbook-Universal Model for Reliability Prediction of Electronic-Components, PCBs and Equipment*, Int. Electro Tech. Commission, Geneva, Switzerland, 2004, pp. 5–10.
[25] *Safety Requirements for Electric Vehicles—Part 3: Protection Against Electric Shock*, document GB/T 18384.3, National Standardization Management Committee, China, 2015, pp. 2–9.
[26] *Drive Motor System for Electric Vehicles—Part1: Specification*, document GB/T18488.2, National Standardization Management Committee, China, 2015, pp. 4–15.
[27] E. A. Elsayed, *Reliability Engineering*, 2nd ed. Beijing, China: Publishing Housing of Electronics Industry, 2012, pp. 99–104 and 45–120.

XIONG SHU received the B.S. degree in mechanical engineering from the Hunan Institute of Science and Technology, Hunan, China, in 2011, and the M.S. degree in mechanical engineering from the Changsha University of Science and Technology, Hunan, in 2014. He is currently pursuing the Ph.D. degree in mechanical engineering with the Hunan University of Science and Technology. He has been engaged in research on new-energy vehicles, since 2012. His research interests include signal processing, fault diagnosis, and reliability analysis techniques of power train system of electric vehicle.

YINGFU GUO received the B.S. and M.S. degrees from Xi'an University of Science and Technology, 1983 and 1989, respectively, and the Ph.D. degree from the China University of Mining and Technology, in 2002. He is currently a Professor of mechanical engineering with the Hunan University of Science and Technology. His research interests include machine condition monitoring, fault diagnosis, reliability analysis, and signal processing.

WENXIAN YANG received the Ph.D. degree in mechanical engineering from Xi'an Jiaotong University, in 1999. Then, he did a research with the City University of Hong Kong, from 2001 to 2002, Nottingham Trent University, from 2002 to 2004, Cranfield University, from 2004 to 2007, the University of Durham, from 2007 to 2009, and the U.K. Offshore Renewable Energy CATAPULT Centre, from 2009 to 2013. In May 2013, he joined Newcastle University as a Lecturer, where he was promoted to Senior Lecturer, in 2018. With the expertise in machine condition monitoring, fault diagnosis, signal processing, pattern recognition, artificial intelligence, system reliability analysis, and reliability design, he has been consistently striving to use advanced condition monitoring and reliability analysis techniques to help the enterprises to increase economic benefits by lowering the downtime and operation and maintenance costs of their production equipment.

KEXIANG WEI received the Ph.D. degree in mechanical engineering from Shanghai Jiaotong University, in 2006. Then, he held a postdoctoral position at Shanghai Jiaotong University for two years. He was invited to the University of Sydney as a Visiting Scholar, from 2010 to 2011. He is currently a Professor of mechanical engineering with the Hunan Institute of Engineering. His research interests include machinery dynamics, vibration control, condition monitoring, and fault diagnosis.

YUN ZHU received the B.S. and M.S. degrees from the Changsha University of Science and Technology, Changsha, China, in 2009 and 2013, respectively, all in mechanical engineering. He is currently a Teacher majoring in automobile engineering with the Hunan Institute of Engineering. His current research interests include electric vehicle energy management, reliability analysis techniques, and energy harvesting.

HONGXIANG ZOU received the B.S. degree from the Huazhong University of Science and Technology, Wuhan, China, in 2001, the M.S. degree from the Changsha University of Science and Technology, Changsha, China, in 2014, and the Ph.D. degree from Shanghai Jiao Tong University, Shanghai, China, in 2017, all in mechanical engineering. He is currently a Distinguished Researcher of Hunan Provincial Key Laboratory of Vehicle Power and Transmission System. His current research interests include smart structure design and dynamic analysis, reliability analysis techniques, and vibration control.